Asymmetry in photocurrent enhancement by plasmonic nanoparticle arrays located on the front or on the rear of solar cells

F. J. Beck,[1,a)] S. Mokkapati,[1] A. Polman,[2] and K. R. Catchpole[1]
[1]*Centre for Sustainable Energy Systems, College of Engineering and Computer Science, Australian National University, Canberra ACT 0200, Australia*
[2]*Center for Nanophotonics, FOM Institute AMOLF, Science Park 104, 1098 XG Amsterdam, The Netherlands*

(Received 2 October 2009; accepted 21 December 2009; published online 22 January 2010)

We show experimentally that there is asymmetry in photocurrent enhancement by Ag nanoparticle arrays located on the front or on the rear of solar cells. The scattering cross-section calculated for front- and rear-located nanoparticles can differ by up to a factor of 3.7, but the coupling efficiency remains the same. We attribute this to differences in the electric field strength and show that the normalized scattering cross-section of a front-located nanoparticle varies from two to eight depending on the intensity of the driving field. In addition, the scattering cross-section of rear-located particles can be increased fourfold using ultrathin spacer layers. © *2010 American Institute of Physics*. [doi:10.1063/1.3292020]

The enhancement of the efficiency of solar cells using plasmonic effects has received a lot of attention in recent years.[1–3] In particular, scattering from subwavelength metal particles is a promising method of providing light-trapping for solar cells.[4–7] Metal nanoparticles can be fabricated on finished solar cells, separated from the semiconductor surface by a dielectric spacer layer which can also serve as a passivation layer. Incident sunlight excites a localized surface plasmon resonance in the nanoparticles, which then couples light into the optically-dense active region of the cell over a broad angular range. A 30% increase in photocurrent across the solar spectrum has been demonstrated using this technique for a 1.25 μm silicon-on-insulator cell using random arrays of Ag nanoparticles.[8]

When nanoparticles are located on the front of a solar cell, destructive interference between incident and scattered light leads to suppressed absorption in the cell at certain wavelengths below the scattering resonance of the nanoparticles.[9] For cells with strong blue response this can lead to an overall decrease in photocurrent across the solar spectrum. To avoid this, nanoparticle arrays with redshifted surface plasmon resonances have been fabricated on the rear of solar cells.[10]

So far, the difference between light scatterings from front- and rear-located particles has not been systematically studied. In this letter, we show clear differences in photocurrent enhancement due to front- and rear-located Ag nanoparticles on thin crystalline Si cells. We demonstrate that this asymmetry is dependent on spacer layer thickness and is the result of differences in the scattering cross-sections of nanoparticles on the front and rear of the Si substrate. We establish a relationship between the strength of the driving field, calculated from an analytical model, and the magnitude of the particle scattering cross-section, for spacer layers thicknesses ranging from 10–45 nm. We report that for ultrathin spacer layers thickness (<10 nm), the scattering cross-section of rear located particles is significantly enhanced. These results constitute important insights for the design of effective light-trapping geometries.

Photocurrent measurements were performed on 20 μm thick, bifacial crystalline Si solar cells, fabricated on p-type, 0.1 Ω cm wafers with 50 Ω cm phosphorous doped emitters and with a dielectric layer structure of 10 nm thermally grown SiO_2 and 8 nm Si_3N_4 grown by low-pressure chemical vapor deposition on both sides. Random Ag nanoparticle arrays were deposited on one side of the cells by thermal evaporation of 16 nm of Ag, followed by a 50 min anneal at 230 °C in N_2 gas. The average diameter of the nanoparticles was 220 nm with a surface coverage of 58%, as determined by scanning electron microscopy. The particles had a "flattened" hemispherical shape with a height of ~30 nm estimated from the surface coverage of the particles and the volume of Ag deposited.

Figure 1 shows the external quantum efficiency (EQE) (number of collected photogenerated carriers per incoming photon), calculated from photocurrent measurements, for a

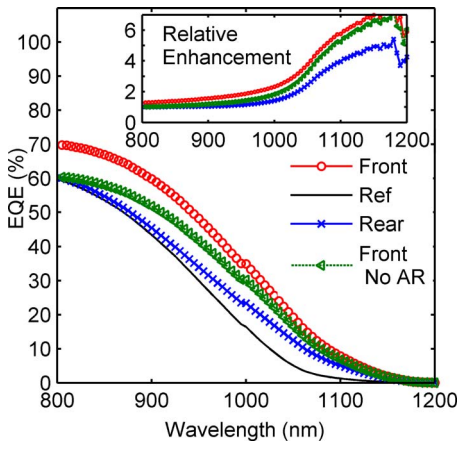

FIG. 1. (Color online) Measured EQE for 20 μm thick c-Si solar cells with Ag nanoparticles on the front (circles) and the rear (crosses) and without nanoparticles (solid line). Additionally, data for particles on the front, corrected for the antireflection effect of the nanoparticles (triangles) is shown. The inset shows the EQE enhancement relative to the reference for all three cases.

a)Electronic mail: fiona.beck@anu.edu.au.

solar cell with nanoparticle layers on the front (circles) or the rear (crosses). Data for the same cell measured without nanoparticles (solid line) is included for reference. The inset shows the EQE enhancement relative to the reference. Figure 1 shows that cells with front-located nanoparticles have 14% (relative) higher EQE than those with no or rear-located particles, at a wavelength of 800 nm where transmission losses are less than 10% (for 20 μm thick Si cells). This is due to the antireflection effect provided by the particles on the front. In contrast, for no or rear-located particles the illuminated surface of the cell will reflect 32% of the incident light at a wavelength of 800 nm. At longer wavelengths the enhancement provided by particles on the front is due to a combination of antireflection and light trapping effects, while for particles on the rear only light trapping contributes. To compare the light trapping effects between front and rear, the data for particles on the front is corrected for the antireflection effect by applying a fixed relative reduction of 14% (triangles in Fig. 1 and inset). Note that this leads to an underestimate of the corrected EQE enhancement, as we would expect the antireflection effect to decrease at wavelengths further away from the scattering resonance wavelength (λ_{SPR}=730 nm, calculated from numerical simulations). It is clear that, for this particular choice of dielectric spacer layer geometry, light trapping by front located nanoparticle arrays provides a larger EQE enhancement than rear-located particles over the spectral range shown.

To investigate the role of the spacer layer in the observed asymmetry in photocurrent enhancement between front- and rear-located nanoparticles, finite-difference time-domain (FDTD) numerical simulations were performed for a single nanoparticle on a Si substrate, using the FDTD solutions package from Lumerical.[11] A simplified geometry was employed, with a single SiO_2 layer between the particle and the substrate, in order to focus the investigation on the effect of spacer layer thickness. Although experimentally nanoparticles of roughly hemispherical shape are observed, a symmetrical disk shape was used; a choice motivated by the fact that for a hemisphere light propagating from the air region encounters a circular convex surface of Ag while from the Si region the light encounters a circular flat Ag surface. Using a disk excludes any effects of shape asymmetry in the modeling and allows us to investigate the physical mechanisms causing asymmetrical behavior.

The normalized scattering cross-section (Q_{scat}) and light coupling efficiency (F_{subs}) of the nanoparticle were calculated using FDTD. The latter is defined as the fraction of light scattered by the nanoparticle that is scattered into the Si. These two quantities give a good measure of the effectiveness of the light trapping provided by the nanoparticle.[3] A 100 nm diameter, 50 nm tall Ag disk was modeled, separated from a semi-infinite Si substrate by a SiO_2 spacer layer of varying thickness. Radiation from the normally incident source was propagated from air into to the substrate (corresponding to nanoparticles on the front) or from the substrate to air (corresponding to nanoparticles on the rear). The dielectric functions were modeled using a Drude model for Ag, fitted to optical data from Johnson and Christy,[12] and a Drude–Lorentz model for Si, fitted to data from Palik.[13] The refractive index of SiO_2 was also taken from Palik. The scattered power was determined by integrating the Poynting vector of the scattered field over a box surrounding the particle.

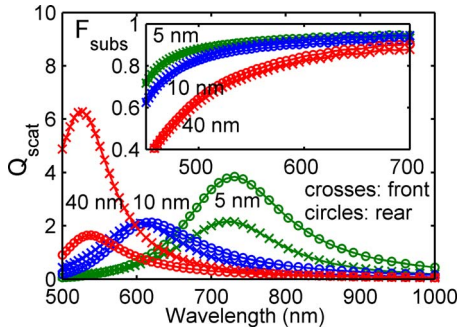

FIG. 2. (Color online) Calculated normalized scattering cross-section (Q_{scat}) and, inset, the fraction of light scattered by the nanoparticle that is scattered into the silicon (F_{subs}), for a Ag disk of diameter 100 nm and height 50 nm, for SiO_2 spacer layer thickness of 5, 10, and 40 nm on a Si substrate. Data is shown for front-(crosses) and rear-(circles) located nanoparticles.

The scattering cross-section was calculated by dividing the scattered power by the incident source power and normalizing the result to the cross-sectional area of the particle.

Figure 2 shows Q_{scat} spectra for Ag nanoparticles on Si substrates with different spacer layer thicknesses of 5, 10, and 40 nm, with particles on the front (crosses) or the rear (circles). The overlap of the particle near-field with the high-index Si substrate causes a redshift of the scattering resonance as the spacer layer thickness reduces.[14] For particles on the front, the normalized scattering cross-section at resonance, $Q_{scat}(\lambda_{SPR})=6.3$ for particles for the 40 nm spacer layer, reducing to $Q_{scat}(\lambda_{SPR})=2.2$ for the thinner spacer layers of 5 and 10 nm. Conversely, for particles on the rear $Q_{scat}(\lambda_{SPR})=3.8$ for the thinnest spacer layer of 5 nm and reduces to a value of 1.7 for the thicker 40 nm case. The inset shows F_{subs} for the same simulations. The coupling efficiency converges to values as high as 90% for the thinnest layers at longer wavelengths, in agreement with previous work on disk-shaped nanoparticles placed close to the substrate.[15] The coupling efficiency is increased as the layers become thinner, which is due to the increased overlap of the near-field with the substrate. No significant difference in coupling efficiency is observed between front and rear simulations. From this result we conclude that the asymmetry in EQE for front- and the rear-located nanoparticles can be attributed to the difference in Q_{scat}.

To investigate the difference in the Q_{scat} spectra of Fig. 2, we consider the time-averaged radiated power of a harmonically oscillating dipole, which is dependent on the square of the dipole moment. In the quasistatic limit the dipole moment is proportional to the driving field $\mathbf{E_d}$, so that $Q_{scat}(\lambda) \sim |\mathbf{E_d}|^2$.[16] We use a simple model to calculate the local driving field at the position of the nanoparticle (i.e., at a position close to the air/dielectric interface), as illustrated in the inset in Fig. 3, taking into account Fresnel reflection in a one-dimensional multilayer geometry excluding the nanoparticle.

For particles on the front, $\mathbf{E_d}$ is a superposition of the incident field ($\mathbf{E_i}$) and the field reflected ($\mathbf{E_r}$) from the air/SiO_2/Si layer structure; for particles on the rear $\mathbf{E_d}$ is equal to the field transmitted through the Si/SiO_2/air layer ($\mathbf{E_t}$). We define $\mathbf{E_i^N}$ as the incident field normalized to the refractive index in each medium, so that the ratio between $\mathbf{E_i^N}$ in the air region, (front-located particles) and in the Si region, (rear-located particles) is equal to n_{Si}, the complex

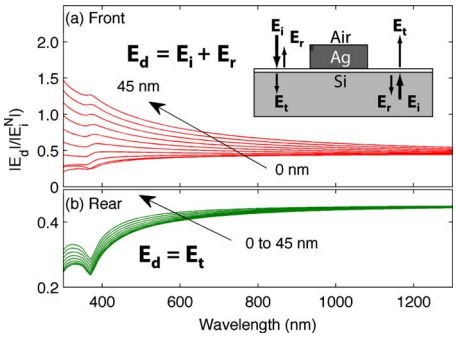

FIG. 3. (Color online) Calculated driving field amplitude $|\mathbf{E_d}|$ relative to the index-normalized incident amplitude $|\mathbf{E_i^N}|$, as a function of wavelength for (a) front- and (b) rear-located Ag nanoparticles on Si for different SiO_2 spacer layer thickness from 0 to 45 nm in steps of 5 nm. The fields are calculated using a one-dimensional transfer matrix method for a planar geometry (see inset) without the nanoparticle.

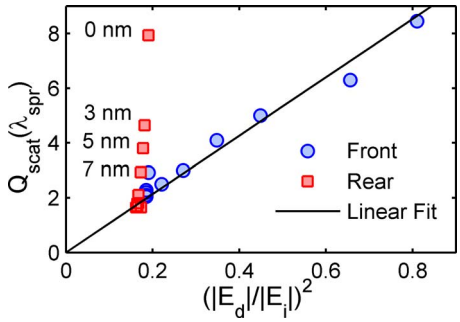

FIG. 4. (Color online) The value of $Q_{scat}(\lambda_{SPR})$, calculated from FDTD simulations, for different spacer layer thicknesses from 0 to 45 nm, plotted against the calculated normalized local field intensity $(|\mathbf{E_d}|/|\mathbf{E_i^N}|)^2$ for front- (circles) and rear-(squares) located particles. A linear fit to the data for front-located particles is also shown.

refractive index of the Si. For particles on the rear, the fields are calculated at the Si/SiO_2 interface, so that absorption into Si does not play a role.

Figure 3 shows $|\mathbf{E_d}|$, relative to the index-normalized incident amplitude $|\mathbf{E_i^N}|$, as a function of wavelength for different spacer layer thicknesses in the range 0–45 nm, for particles on the front (a) and the rear (b). The normalized driving field increases with spacer layer thickness for particles on both the front and rear of the Si substrate. For particles on the front, $\mathbf{E_d}$ is at a minimum when no spacer layer is present as $\mathbf{E_i}$ and $\mathbf{E_r}$ destructively interfere due to the phase shift on reflection. The spacer layer introduces an extra phase lag between $\mathbf{E_i}$ and $\mathbf{E_r}$, which increases with the thickness of the spacer layer and which is more pronounced at short wavelengths where the path length in the spacer layer is significant relative to the wavelength. This extra phase shift reduces the destructive interference between $\mathbf{E_i}$ and $\mathbf{E_r}$, hence $\mathbf{E_d}$ increases with the spacer layer thickness for particles on the front. For particles on the rear, the additional phase shift introduced by the spacer layer results in constructive interference between multiply scattered fields, leading to a slightly higher driving field for larger layer thicknesses.

From Fig. 3, we can compare $|\mathbf{E_d}|/|\mathbf{E_i^N}|$ for substrates with 40 nm spacer layers, calculated at $\lambda_{SPR}=530$ nm, for front-located $(|\mathbf{E_d}|/|\mathbf{E_i^N}|=0.81)$ and rear-located particles, $(|\mathbf{E_d}|/|\mathbf{E_i^N}|=0.42)$. The ratio of driving field intensities, $(0.81/0.42)^2=3.7$, while the corresponding ratio of $Q_{scat}(\lambda_{SPR})$ (from Fig. 2) is 3.9.

In Fig. 4 we present values of $Q_{scat}(\lambda_{SPR})$, derived from FDTD simulations for several spacer layer thicknesses in the range 0–45 nm, plotted against the corresponding $(|\mathbf{E_d}|/|\mathbf{E_i^N}|)^2$. A clear correlation between $Q_{scat}(\lambda_{SPR})$ and $(|\mathbf{E_d}|/|\mathbf{E_i^N}|)^2$ is observed for particles on the front for the spacer layer thickness range studied. Similarly, good correlation is found for rear-located particles for spacer layer thicknesses above 10 nm. However, for rear-located nanoparticles with spacer layers of less than 10 nm, $Q_{scat}(\lambda_{SPR})$ increases rapidly as the spacer layer thickness reduces. Numerical simulations for this geometry show a high field concentration in the substrate near the particle at the scattering resonance; this is not observed for front-located nanoparticles. Further research to study this is underway.

Returning to the experimental geometry of the solar cell measured in Fig. 1, we can calculate the square of the driving field for particles on the front, $(|\mathbf{E_d}|/|\mathbf{E_i}|)^2=0.21$, and on the rear, $(|\mathbf{E_d}|/|\mathbf{E_i}|)^2=0.18$ at $\lambda_{SPR}=730$ nm. The ratio of driving field intensities is, therefore, 1.2 for the experimental case. Based on these calculations, we attribute the larger EQE enhancements measured for solar cells with front-located nanoparticles (triangles from inset in Fig. 1), compared with rear-located nanoparticles (crosses), to a roughly 20% larger $Q_{scat}(\lambda_{SPR})$ for front-located particles due to the difference in driving field.

In summary, we have shown that optimizing the driving field is important to achieve strong scattering from Ag nanoparticles for light-trapping applications in solar cells. The driving field increases with dielectric spacer layer thickness and should be considered separately for particles on the front and the rear of a solar cell. Very thin spacer layers (<10 nm) enhance the magnitude of the scattering cross-section for rear-located particles due to an additional effect that will be the focus of further work.

This work is financially supported by the Australian Research Council and the Foundation for Fundamental Research on Matter (FOM) which is supported by NWO, as part of the Joint Solar Program.

[1]H. A. Atwater and A. Polman, Nature Mater. (to be published).
[2]S. Hayashi, K. Kozaru, and K. Yamamoto, Solid State Commun. **79**, 763 (1991).
[3]K. R. Catchpole and A. Polman, Opt. Express **16**, 21793 (2008).
[4]D. Derkacs, S. H. Lim, P. Matheu, W. Mar, and E. T. Yu, Appl. Phys. Lett. **89**, 093103 (2006).
[5]C. Hägglund, Z. Zach, G. Petersson, and B. Kasemo, Appl. Phys. Lett. **92**, 053110 (2008).
[6]K. Nakayama, K. Tanabe, and H. A. Atwater, Appl. Phys. Lett. **93**, 121904 (2008).
[7]D. M. Schaadt, B. Feng, and E. T. Yu, Appl. Phys. Lett. **86**, 063106 (2005).
[8]S. Pillai, K. R. Catchpole, T. Trupke, and M. A. Green, J. Appl. Phys. **101**, 093105 (2007).
[9]S. H. Lim, W. Mar, P. Matheu, D. Derkacs, and E. T. Yu, J. Appl. Phys. **101**, 104309 (2007).
[10]F. J. Beck, A. Polman, and K. R. Catchpole, J. Appl. Phys. **105**, 114310 (2009).
[11]Lumerical FDTD Solutions, www.lumerical.com
[12]P. B. Johnson and R. W. Christy, Phys. Rev. B **6**, 4370 (1972).
[13]E. D. Palik, *Handbook of Optical Constants of Solids* (Academic, New York, 1998).
[14]G. Xu, M. Tazawa, P. Jin, and S. Nakao, Appl. Phys. A: Mater. Sci. Process. **80**, 1535 (2005).
[15]K. R. Catchpole and A. Polman, Appl. Phys. Lett. **93**, 191113 (2008).
[16]C. F. Bohren and D. R. Huffman, *Absorption and Scattering of Light by Small Particles* (Wiley-VCH, Weinheim, 2004).